# Nature of Dark Energy and Polarization Measurements

R. Mainini [1], L.P.L. Colombo [2] & S.A. Bonometto [3]

*Physics Department G. Occhialini, Università degli Studi di Milano–Bicocca, Piazza della Scienza 3, I20126 Milano (Italy)*

*I.N.F.N., Via Celoria 16, I20133 Milano (Italy)*

**Abstract**

High sensitivity polarization measures, on wide angular scales, together with data on anisotropy, can be used to fix DE parameters. In this paper, first of all, we aim to determine the sensitivity needed to provide significant limits. Our analysis puts in evidence that there is a class of DE models that polarization measures can possibly exclude soon. This class includes models with DE due to a Ratra–Peebles (RP) potential. Using a likelihood analysis, we show that it is possible to distinguish RP models from ΛCDM and other dynamical DE models, already with the sensitivity of experiments like SPOrt or WMAP, thanks to their negative $TE$ correlation at low–$l$, when the optical depth $\tau$ is sufficiently large. On the contrary, fixing the energy scale $\Lambda$ for RP potentials or distinguishing between ΛCDM and other DE potentials requires a much lower pixel noise, that no planned polarization experiment will achieve. While reviewing this paper after the referee report, the first–year WMAP data were released. WMAP finds large positive anisotropy–polarization correlations at low $l$; this apparently excludes DE models with RP potentials.

*Key words:* Cosmic Microwave Background, Cosmology: Cosmological Parameters
*PACS:* 98.70.Vc, 98.80.-k

## 1 Introduction

The nature of Dark Energy (DE) is one of the main puzzles of modern cosmology. DE was first required by SNIa data (see, e.g., Perlmutter et al. 1998,

[1] E-mail: roberto.mainini@mib.infn.it
[2] E-mail: loris.colombo@mib.infn.it
[3] E-mail: silvio.bonometto@mib.infn.it

Riess et al. 1998), that indicate an accelerated cosmic expansion. A flat Universe with $\Omega_m \simeq 0.3$ and $\Omega_b h^2 \simeq 0.02$ is also favored by an analysis of CMB and LSS observations (see, e.g., Tegmark et al., 2001; Netterfield et al, 2002; Percival et al., 2002; Efstathiou et al, 2002; Schuecker et al., 2003; Pogosian et al.,2003; here $\Omega_{m,b}$: matter, baryon density parameters; $h$: Hubble parameter in units of 100 km/s/Mpc; CMB: cosmic microwave background; LSS: large scale structure).

The cosmic component allowing flatness, in spite of $\Omega_m \simeq 0.3$, should not be observable in the number–of–particle representation, in the present epoch. If this component is a false vacuum, whose pressure and energy density ($p_{DE}$ and $\rho_{DE}$) have ratio $w = -1$, a severe fine tuning of $\rho_{DE}$, at the end of the electroweak transition, is required; in fact, before it, the vacuum energy density could be more than $10^{50}$ times greater than now. A possible alternative, apparently reducing fine tuning requirements, is that DE arises from a self–interacting scalar field $\phi$ (dynamical Dark Energy or *quintessence*; see, e.g., Ratra–Peebles 1988, RP hereafter; Wetterich 1988, 1995; Ferreira & Joyce 1998; Perrotta & Baccigalupi 1999; Steinhardt et al. 1999; Zlatev et al. 1999; Albrecht & Skordis 2000; Amendola 2000; Brax, Martin & Riazuelo 2000). For dynamical DE,

$$\rho_{DE} = \frac{\dot{\phi}^2}{2a^2} + V(\phi) \quad , \qquad p_{DE} = \frac{\dot{\phi}^2}{2a^2} - V(\phi), \tag{1.1}$$

$V(\phi)$ being the self–interaction potential, $a$ is the scale factor and dots indicate derivatives in respect to the conformal time $t$. The ratio $w$ becomes negative as soon as $\rho_k = \dot{\phi}^2/2a^2 < V$. For $\rho_k/V \simeq 1/2$, it is $w \simeq -1/3$ and dynamical DE approaches open CDM. Still smaller $\rho_k/V$ ratios allow to approach $w = -1$ and a $\Lambda$CDM behavior. In order to work out $w$ and its time variations, Friedman equations, in association with the equation of motion of $\phi$, are to be integrated.

Solutions clearly depend on the shape of $V$, which, in principle, is largely arbitrary. However, among potentials admitting a *tracker* solution, a particular relevance is kept by RP and SUGRA (Brax & Martin 1999, 2000) expressions

$$V(\phi) = \Lambda^{4+\alpha}/\phi^{\alpha} \ , \qquad V(\phi) = (\Lambda^{4+\alpha}/\phi^{\alpha}) \exp(4\pi\phi^2/m_p^2) \ , \tag{1.2}$$

which originate within the frame of Supersymmetric (SUSY) theories. In the expressions (1.2), $m_p$ is the Planck mass and $\Lambda$ is an energy scale, currently set in the interval $10^2$–$10^{10}$ GeV, ranging between the electroweak scale and the SUSY soft breaking scale. The potentials (1.2) also depend on the exponent $\alpha$; once $\Lambda$ and $\Omega_{DE}$ are assigned, however, $\alpha$ is univocally determined. The RP and SUGRA potentials are also indicative of the opposite cases, when $w$ shows slow or fast time variations, respectively.

Dynamical DE and ΛCDM predict quite similar observational results, in most cases. This is a point in favor of dynamical DE, as it is known that ΛCDM allows a good fit of most available data. It is however important to devise suitable experiments whose outputs enable us to probe DE nature; if DE is dynamical, they should also enable us to fix the expression of $V$ and the values of the parameters on which $V$ depends.

Here we show that measures of anisotropy and polarization of CMB at large angular scales can constrain $V$. If favorable (but not exceptional) conditions are fulfilled, polarization measures, at a sensitivity level comparable with experiments in progress, can provide significant information, possibly *excluding* that a RP potential describes DE.

We shall show this point by performing a likelihood analysis, assuming that polarization measures come from an experiment similar to the Sky Polarization Observatory (SPOrt: see, e.g., Macculi et al, 2000; Carretti et al, 2000; Peverini et al, 2001), considering both a noise level that the experiment will attain and a lower noise level, as well. Our results, however, are not directly related to the above experiment and can be easily extrapolated to other observational contexts.

## 2 The cosmic opacity to CMB photons

In the present cosmic epoch, although diffuse baryonic materials are almost completely ionized, the scattering time for CMB photons $t_s \simeq 4.45{\cdot}10^{18}\Omega_b^{-1}h^{-2}$s exceeds the Hubble time $t_H = 3.09 \cdot 10^{17}h^{-1}$s and the Universe is transparent to CMB photons. These figures can be extrapolated to the past, but, while $t_s \propto a^3$, the dependence of $t_H$ on $a$ depends on the cosmological model. In an expansion regime dominated by non–relativistic matter, a fully ionized Universe is opaque to CMB at redshifts $z > z_{op} \simeq 5\,(\Omega_b h)^{-2/3}$. Therefore, assuming $\Omega_b h^2 \simeq 0.022$ (standard BBNS limits; see, e.g., Dolgov 2002 for a recent review) and $h \simeq 0.5$–$0.7$, we have $z_{op} > 64$, safely above any expected value for the reionization redshift $z_{ri}$. No reasonable cosmological model allows a substantial reduction of such $z_{op}$.

While, therefore, $\tau \ll 1$, its specific value depends on the model and, in particular, on the reionization history. If reionization is a single and sudden event, it can be synthesized by a value of $z_{ri}$. In Fig. 1 we show how $\tau$ is related to $z_{ri}$, for a wide set of cosmological models. In general, $z_{ri} \sim 8$ or $\sim 16$, if we require $\tau = 0.08$ or $0.16$.

Data can constrain the reionization history in indirect ways. High–$z$ QSO spectra (Djorgovski et al. 2001; Becker et al. 2001) show that at least a fraction

of neutral hydrogen is present, in the intergalactic medium, at $z \gtrsim 6$. These very authors, however, warn the reader against an immediate conclusion that $z_{ri} \simeq 6$; an ionization rate $x \sim 0.01$ can cause the Gunn–Peterson effect observed. Their finding, however, was taken as an indication of the expected range of $z_{ri}$.

Another constraint can be found, if the ionizing flux observed today is extrapolated to high $z$; in this way, Miralda–Escudè (2002) found that that the photon flux is able to reionize the cosmic hydrogen at $z_{ri} \sim 8$–$10$ and $\tau \simeq 0.08$.

Pushing farther the theoretical analysis, Tegmark (1997) estimated that, at $z \simeq 30$, a fraction $\sim 10^{-3}$ of baryonic matter is in fluctuations of $\sim 10^2$–$10^3 M_\odot$, already in non–linear growth. They can cool and turn into massive stars thanks to molecular hydrogen radiation. However, as soon as thermonuclear processes ignite, stars produce photons hard enough to turn all hydrogen into atomic (or plasma) state and star formation is stopped until much greater fluctuations ($\sim 10^7 M_\odot$) enter a non–linear regime (see, e.g., Haiman 1997, Gnedin & Ostriker 1997). However, Haiman et al. (2000), Oh (2001) and Venkatesan et al. (2001) find that the situation can be even more complicated, as X–ray heating might enhance the formation of molecular hydrogen. From such pictures, Cen (2002) and Whyithe & Loeb (2002) try to deduce the reionization history. According to them, when the first PopIII stars form, a first high–$z$ reionization occurs. PopIII stars eventually produce metals that, in turn, allow less massive stars to form and, therefore, the ionizing photon flux is reduced soon. Then the overall ionization rate is set by a balance between star formation and hydrogen recombination; the former overwhelming the latter at a redshift $\sim 8$, when $x$ safely approaches unity. At such redshift, this picture meets Miralda–Escudè (2002) conclusions and is therefore also coherent with the ionizing flux observed today.

These pictures are qualitatively realistic, although their quantitative aspects are still uncertain. It should be emphasized that different reionization histories, also when they yield the same $\tau$, give different CMB angular spectra. In this work we shall quantitatively explore simple reionization histories, where a single reionization event yields $\tau = 0.08$ or $0.16$ and comment on the extension of our results to more complex histories. The former $\tau$ value agrees with Miralda–Escudè (2002) estimate. The latter value assumes an earlier reionization, implicitly allowing a small hydrogen fraction ($\sim 1\,\%$) to remain neutral until $z \sim 6$, to account for the observed Gunn–Peterson effect in high–$z$ QSO spectra.

It should also be reminded that, until CMB spectra analysis is restricted to anisotropy data, no significant constraint on $\tau$ can be set; Stompor et al (2002), using balloon data, can only set the limit $\tau < 0.40$, at the $2$–$\sigma$ level. Limits are so loose because of the degeneracy between $\tau$ and $n$ (primeval spectral

index), in CMB anisotropy data. In a recent paper, Colombo & Bonometto (2003) discussed how much such degeneracy can be removed using polarization measures. Recent observations (Kovac et al. 2002) apparently confirmed that CMB is polarized, but the sensitivity level and the angular scales probed by such observations were not adequate to reduce the above $n$–$\tau$ degeneracy.

In this work we explore what large angular scale CMB polarization data can tell us on DE nature. For the sake of simplicity, we assume that all model parameters are obtained from measures at smaller angular scales and concentrate on the effect of the potential $V(\phi)$ on large angular scales, when $\tau$ is large.

## 3 CMB angular spectra

The linear evolution of density fluctuations in models with a DE component yields the angular spectra $C_l^A$; $A = T,\ E,\ B,\ X$ stand for anisotropy, $E$– and $B$–mode polarization and anisotropy–polarization cross correlation (X=TE) only $E$–mode polarization is considered through this paper. In Fig. 2–5 we show the spectra $C_l^{T,X,E}$ when the potential is RP or SUGRA and $\tau$ is 0.08 or 0.16, for a set of values of the energy scale $\Lambda$. All spectra are obtained with suitable extensions of CMBFAST [4] .

Figs. 2 to 5 show that the nature of DE and, in particular, the value of the energy scale $\Lambda$, both for RP and SUGRA models, display their main effects on low–$l$ TE correlation spectra. In particular, Figs.2 and 3 show that $C_l^X$ is negative, at low $l$, for RP potentials, while, in SUGRA models, such feature is absent. Negative $C_l^X$ are not an exceptional feature: all models yield alternate intervals of positive and negative $C_l^X$ as $l$ increases. In most spatially flat models, however, the $C_l^X$ spectrum, at low $l$ values, starts from positive values. On the contrary, open CDM models, when $\tau$ is large enough, start with negative $C_l^X$, al low $l$.

In the discussion section, we shall discuss why RP models share this feature with open models. This arises from the way how $\rho_{DE}$ scales with $a$, similar to the scaling of the curvature term in open models. On the contrary, in $\Lambda$CDM models, $\rho_{DE}$ does not depend on $a$. When the scaling of $\rho_{DE}$ with $a$ is mild and, therefore, close to $\Lambda$CDM, no low–$l$ negative $C_l^X$ is expected.

[4] `http://physics.nyu.edu/matiasz/CMBFAST/cmbfast.html`

## 4 Likelihood analysis

### *4.1 The SPOrt experiment*

In this section we aim to determine the likelihood of different models in respect to possible results of anisotropy and polarization measurements, obtained through definite observational apparati, for specific cosmological models. In particular, polarization data sets are built with reference to the features of the SPOrt experiment.

At variance from other space experiments (WMAP and PLANCK), SPOrt has been explicitly designed to measure the Stokes parameters Q and U and to minimize systematics and instrumental polarization. SPOrt will observe a sky area with declination $|\delta| \leq 51.6^o$ ($\sim 80\%$ of the whole sky). The lifetime of the experiment will be at least 1.5 years, but an extension is likely.

Here we assume that pixels are distributed according to the HEALPix [5] package, with $N^{side} = 16$, and smoothed with a Gaussian beam of FWHM of $7^o$. We therefore have, on the whole sky, 3072 pixels, whose centers lie at an average angular distance of $\sim 3.7^o$. Once polar caps are excluded, there remain 2448 pixels, providing measures of the Stokes parameters $Q$ and $U$.

SPOrt polarimeters will provide no anisotropy data. Such information will be however available through other experiments (COBE, WMAP). Of course, anisotropy data probe a different sky area, i.e. the whole sky, excluding the area with galactic declination $|\delta| < 20^o$, where contamination by the Milky Way is severe. (On the contrary, such contamination can be assumed to be under control, for polarization data; see, e.g., Bruscoli et al. 2002; Tucci et al. 2002.) In this sky area there are 1984 pixels. For 1360 of them, both anisotropy and polarization data are supposed to be available.

Random noise ($\sigma^P_{pix}$) is included in artificial data, assuming it to be uncorrelated, both among pixels and between $Q$ and $U$, in the case of polarization measures. We assume $\sigma^T_{pix} = 1\,\mu$K for temperature data (as expected for WMAP measurements, extended to 4 years, scaled to the SPOrt resolution). On the contrary, we consider different noise levels for polarization data.

At present, the SPOrt experiment team expects a pixel noise level of

$$\sigma^P_{pix} \simeq 1.8\,\frac{N^{side}}{8}\,\sqrt{\frac{2}{\lambda}\frac{0.6}{\epsilon}}\;\mu\mathrm{K},$$

where $\lambda$ is the experiment's lifetime in years while $\epsilon$ indicates the detection efficiency. Our analysis considers $\sigma^P_{pix}$'s in the interval comprised from 0.1 to

[5] `http://www.eso.org/science/healpix/`

$1\,\mu$K per pixel. Even at its highest value, this noise is consistent with SPOrt claims only if $\lambda = 4\,y$ and efficiency approaches unity. However, the SPOrt payload is to be delivered in more than one year and there is room for some further improvement in the apparati.

### *4.2 Models explored*

In this analysis we take $\Omega_{DE} = 0.7$, $\Omega_b h^2 = 0.022$, $h = 0.7$ and a primeval spectral index $n = 1$. We considered also different values for these parameters, but the likelihood distributions are essentially independent from them. On the contrary, such distributions depend on the choice of $\tau$; as already outlined, we studied likelihood distributions for $\tau = 0.08$ and $0.16$.

We consider first RP models, for $\Lambda/\mathrm{GeV} = 10^3$ and $10^6$. As is known, RP models are accelerated only if $\Lambda \lesssim 10^4$GeV and disagree with SNIa data at the $2$–$\sigma$ level, when $\Lambda \gtrsim 10^6$GeV. On the contrary, when $\Lambda \lesssim 1\,$GeV, the angular spectra of the model are hardly distinguishable from $\Lambda$CDM. Accordingly, fits yielding $\Lambda \lesssim 1\,$GeV, for a RP model, indicate that data do not allow to appreciate that the model is different from $\Lambda$CDM.

We consider then SUGRA models, for $\Lambda/\mathrm{GeV} = 10^3$, $10^6$ and $10^9$. Their $TE$ correlation spectra show differences from $\Lambda$CDM and among themselves, although not so relevant as for RP.

$TE$ correlation spectra also depend on the reionization history. In this paper, such dependence is not explored and this is the main quantitative limitation to the results shown here.

Dealing with low $l$'s, cosmic variance must be carefully taken into account. We explore this point by simulating and analyzing a large number of artificial data sets. Results will be both synthesized into average predictions and analyzed providing the frequency of possible determinations.

### *4.3 Results*

We report first results for RP models, for $\Lambda/\mathrm{GeV} = 10^3$ and $10^6$. In Figs. 6 and 7 we show the average likelihood distributions for such models. In Figs. 8 and 9, we report the distributions of the 1–2 $\sigma$ lower limits on $\Lambda$, for $\tau = 0.08$ and $0.16$, $\Lambda = 10^3$ and $10^6$, $\sigma^P_{pix} = 0.1\,\mu$K and $1\,\mu$K.

Fig. 10 is analogous to Fig. 6, but concerns a SUGRA model with $\Lambda = 10^9$GeV and $\tau = 0.16$; among the cases considered here, this is the one which allows

the best recovery of $\Lambda$. In Fig. 11, we report the distributions of the lower limits on $\Lambda$ for such model (at $1\,\sigma$).

The above figures show that the energy scale $\Lambda$ cannot be detected for SUGRA models, at least with large–angular–scale experiments. This is not only true at a noise level achievable by SPOrt, but also when noise is reduced by a factor $\sim 10$.

The situation was better for RP models. The capacity of an experiment to distinguish a RP model from $\Lambda$CDM increases with the energy scale $\Lambda$ and the opacity $\tau$, although being more sensitive to the former parameter. In fact, a substantial fraction of realizations, with $\Lambda = 10^6$GeV and $\tau = 0.08$, can be distinguished from $\Lambda$CDM, even at the 3–$\sigma$ level; such fraction is only slightly greater for $\tau = 0.16$. Furthermore, only in quite a small fraction of realizations, RP cannot be distinguished from $\Lambda$CDM, at the 2–$\sigma$ level. Both with $\tau = 0.08$ and 0.16, also models with $\Lambda = 10^3$GeV can be distinguished from $\Lambda$CDM in a smaller (but still substantial) fraction of realizations, at least at the 2–$\sigma$ level.

If we aim farther and try to determine $\Lambda$, we meet substantial difficulties: even reducing the noise level by a factor $\sim 10$, the best we can find is a lower limit on the order of magnitude of $\Lambda$. Unfortunately, this can be fixed just in a fraction of realizations.

## 5 Discussion

Let us first discuss how the likelihood distribution can be obtained from the spectra of a given model, taking into account that the number of pixels for anisotropy and polarization ($N_T$ and $N_P$) in our (artificial) data are however different. Let then $T_j$ be the anisotropy measured in $N_T$ pixels and $Q_j$ and $U_j$ the Stokes parameters measured in $N_P$ pixels. In general, let us define vectors $\mathbf{x} \equiv (T_1, ....., T_{N_T}, Q_1, ....., Q_{N_P}, U_1, ....., U_{N_P})$, of $N_s = N_T + 2N_P$ components, defining an observed state of anisotropy and polarization. Once a $\Lambda$ value is assigned, the angular spectra $C_l^A = (C_l^T, C_l^E, C_l^X)$ are univocally determined. On the contrary, a data vector $\mathbf{d}$, of $N_s$ components, built from them, is just a *realization* of such model: once the $N_s$ component vector $\mathbf{d}$ is assigned, the value of $\Lambda$ is not univocally fixed.

A function

$$L(\mathbf{d}|C_l^A) \propto [\det \mathbf{M}]^{-\frac{1}{2}} \exp[-\frac{1}{2}\mathbf{d^T}\mathbf{M}^{-1}\mathbf{d}] \qquad (5.1)$$

is then built, to yield the likelihood of a given set of $C_l^A$ (i.e., of a given $\Lambda$ value), if $\mathbf{d}$ is observed. The main ingredient of $L$ is the correlation matrix $\mathbf{M_{ij}} = \langle \mathbf{x}_i^T \mathbf{x}_j \rangle = \mathbf{S}_{ij} + \mathbf{N}_{ij}$; here $\mathbf{S}_{ij}$ is the signal term and $\mathbf{N}_{ij}$ is due to

the noise. The components $\mathbf{M_{ij}}$ yield the correlation between the $i$th and $j$th elements of data vectors $\mathbf{x}$ corresponding to particular choices of $C_l^A$, i.e. of $\Lambda$ values. The construction of the (model dependent) signal term, however, does not require to build explicitly the vectors $\mathbf{x}$. The procedure to be followed, in the case when both anisotropy and polarization data are available, is explicitly reported by Zaldarriaga (1998). The construction of the noise term is simpler, as we expect no noise correlation, and the matrix $\mathbf{N}_{ij} = \delta_{ij}\,{\sigma_{T,pix}}^2$ (for $i = 1, ..., N_T$) and $\mathbf{N}_{ij} = \delta_{ij}\,{\sigma_{P,pix}}^2$ (for $i = N_T + 1, ..., N_s$) is diagonal.

In what follows, the technical role of the $C_l^A$ spectra does not need to be further outlined and the likelihood function is explicitly considered to depend on $\Lambda$. In particular, we assume that the most probable $\Lambda$ value, for a given anisotropy–polarization state $\mathbf{d}$, is the one which maximizes the likelihood. By integrating the likelihood distribution along the $\Lambda$ axis, we are then able to find the intervals corresponding to 1–2–3 $\sigma$ levels.

In order to explore cosmic variance, 1000 realizations of each model were considered; the likelihood curves plotted in the Figs. 5–6–7–11 are averages of the results of such realizations. 1–2–3 $\sigma$ value distributions, instead, allow to appreciate the spread among the results of each such realization.

The feature which explains why RP model likelihoods can enable us to distinguish them from $\Lambda$CDM, in several cases, is the negative TE correlation at low $l$. In the case of SUGRA models such TE anticorrelation is absent and large angle data seem unsuitable to provide information on DE nature.

Negative TE correlations are essentially related to the simultaneous action of ISW effect and cosmic opacity. The former effect is a consequence of the varying rate of expansion, when we pass from matter to curvature dominance, in open models, or from matter to vacuum dominance in $\Lambda$CDM models. However, while the former kind of passage, in the presence of cosmic opacity, does produce anticorrelation, the latter kind of passage does not.

The capacity of RP models to induce anticorrelation, as we shall see, is related to their features, which more closely approach open CDM, rather than $\Lambda$CDM. The opposite is true for SUGRA models.

A full understanding of model dynamics requires that the whole set of Boltzmann equations, describing photon distribution, is followed in time. Such equations are shown in a number of papers, together with equations ruling the dynamics of fluctuations in other components of a model (see, e.g., Ma & Bertschinger 1995). Signs and other definitions that we adopt here are the same as in the public code CMBFAST. Let us then indicate by $F_l(k,t)$ and $G_l(k,t)$ the Boltzmann components for anisotropy and polarization, respectively, $k$ and $t$ being the wave–number and the conformal time.

Let then $n_e$ and $\sigma_T$ be the free electron density and the Thomson cross–section. The opacity to CMB photons reads then $\tau = \int_t^{t_o} n_e(t')\sigma_T a(t')\, dt'$ and $-\dot{\tau} = a\, n_e \sigma_T$.

Let us report then the set of equations fulfilled by the $G_l$ components in spatially flat models:

$$\dot{G}_l = -\dot{\tau}[-G_l + \frac{\Pi}{2}(\delta_{l0} + \frac{\delta_{l2}}{5})] + \frac{k}{2l+1}[l\, G_{l-1} - (l+1)G_{l+1}] \qquad (5.2f)$$

($\delta_{ln}$ is the Kronecker symbol). Here

$$\Pi = G_o + G_2 + F_2, \qquad (5.3)$$

is the only vehicle transferring signals from anisotropy to polarization.

In a non-flat geometries eq. (5.2f) becomes

$$\dot{G}_l = -\dot{\tau}[-G_l + \frac{\Pi}{2}(\delta_{l0} + \frac{\delta_{l2}}{5})] + \frac{\beta}{2l+1}[l b_l\, G_{l-1} - (l+1)b_{l+1}G_{l+1}]\ ; \quad (5.2o)$$

here $\beta^2 = k^2 + K$ and $b_l^2 = 1 - Kl^2/\beta^2$, with $K = -(1-\Omega_m)H_0^2$, $H_0$ being the present value of the Hubble parameter.

Quite in general, when $n_e$ and, therefore, $-\dot{\tau}$ is large, all $G_l$ are exponentially damped. On the contrary, when $n_e$ is low, the polarization signal spreads along the $G_l$ component series.

In order to produce polarization, therefore, there must however be a seed coming from anisotropy, linked to the non–vanishing of the quadrupole term $F_2(k,t)$. If $F_2(k,t)$ becomes significant only when $n_e$ is very low, little polarization is produced on harmonics with $l$ corresponding to such $k$. It is so for wavelengths $2\pi/k$ entering the horizon well after recombination, which correspond to spectral components with $l \ll 200$, unless reionization occurs. This explains the sudden rise of $C_l^P$ in Fig. 2–5, when $\tau > 0$ is considered.

Let $F_l^o$ ($G_l^o$) be the value taken by $F_l$ ($G_l$) at the present time $t_o$. In spatially flat models, the angular spectra read

$$C_l^T = \frac{\pi}{4}\int d^3k\, P_o(k)\ |F_l^o(k)|^2\ ,\quad C_l^P = \frac{\pi}{4}\int d^3k\, P_o(k)\, |G_l^o(k)|^2\ ,$$

$$C_l^X = \frac{\pi}{4}\int d^3k\, P_o(k)\, F_l^o(k) G_l^o(k)\ , \qquad (5.4f)$$

$P_o(k)$ being the primeval fluctuation spectrum. In open model, angular spectra expressions are slightly more complex and read

$$C_l^T = \frac{\pi}{4}\int d^3\beta\, P_o(q)\ |F_l^o(\beta)|^2\ ,\quad C_l^P = \frac{\pi}{4}\int d^3\beta\, P_o(q)\, |G_l^o(\beta)|^2\ ,$$

$$C_l^X = \frac{\pi}{4} \int d^3\beta \, P_o(q) \, F_l^o(\beta) G_l^o(\beta) \; ; \qquad (5.4o)$$

here $q = (\beta^2 - 4K)^2/\beta(\beta^2 - K)$. Clearly, for $\Omega_m = 1$, both $\beta$ and $q$ return $k$.

Both eqs. (5.2) and (5.4) indicate the presence of suitable shifts in the $k$–space, when open models are considered. In particular, the $b_l$ coefficients in eq. (5.2o) are responsible for the shifts of $C_l$ peaks, while the shifts due to the passage from $k$ to $\beta$ and $q$, in eq. (5.4o), displace the power of the spectrum $P_o$ through the harmonics $F_l$ at small $l$, i.e. on scales comparable with the curvature scale.

Apart of these geometric and power shifts, the main difference between flat and open models resides in the equation fulfilled by the gravitational field fluctuations $\dot{h}$ and $\eta$. In the synchronous gauge, for open models:

$$2\bar{k}^2\dot{\eta} = 8\pi G a^2 [\sum_c (\rho_c + p_c)\theta_c - \dot{h}\rho_{o,cr}(1 - \Omega_m)/a^2]; \qquad (5.5o)$$

here $\rho_{o,cr}$ being the critical density at $z = 0$ and $\sum_c$ indicates a sum over all (relativistic or non–relativistic) matter components. In the same gauge, for flat models with DE:

$$2k^2\dot{\eta} = 8\pi G a^2 [\sum_c (\rho_c + p_c)\theta_c + (\rho_{DE} + p_{DE})\theta_{DE}], \qquad (5.5f)$$

where the DE term has been set in evidence, with its possible fluctuations. The wave–numbers $\bar{k}^2$ and $k^2$ are shifted by $3K$. Once again this corresponds to a shift in the $k$–space.

Let us notice soon that, in a $\Lambda$CDM model, no DE fluctuations exist and, furthermore, $\rho_{DE} = -p_{DE}$, so that the second term at the r.h.s. of eq. (5.5f) vanishes.

In models with dynamical DE, instead, $\theta_{DE}$ does not vanish and, in general, $\rho_{DE} \neq -p_{DE}$. Accordingly, the second term in square brackets in eq. (5.5f) may read $\theta_{DE}\rho_{o,cr}(1-\Omega_m)(1+w)(\rho_{DE}/\rho_{o,DE})$ (the ratio in the last parenthesis tells us how DE energy scales with $a$). This term is then analogous to the second term in square bracket in eq. (5.5o). It would coincide with it if $w = -1/3$ and, namely, if $\theta = -\dot{h}/2$. If the latter is true, we can expect that, apart of a different power distribution along the $l$ axis and geometric effects at greater $l$, there can be specific similarities in the behavior of open and dynamical DE models.

The relation between $\dot{h}/2$ and $\theta_{DE}$ can be studied through the equation

$$\theta_{DE} + \frac{\dot{h}}{2} = -\frac{1}{1+w} [\dot{\delta}_{DE} + 3\frac{\dot{a}}{a}(c_s^2 - w)\delta_{DE}], \qquad (5.6)$$

whose validity indicates that DE behaves as a fluid; here $c_s$ is the sound velocity in DE. This equation can be derived from the equation of motion of

$\phi$, as shown in Appendix A. An order of magnitude estimate, however, tells us soon that $\theta_{DE} \sim k^2 t\, \delta_{DE}$; then, the ratio between $\theta_{DE}$ and the r.h.s. is $\sim (t/L)^2$, where $L$ is the scale related to $k$. When $t \ll L$ (before horizon crossing), the $\theta_{DE}$ term is negligible, in comparison with the r.h.s.. For $L \ll t$ (after horizon crossing), the contrary is true. Hence, before horizon crossing, $\dot{h}/2$ is essentially required to equate the r.h.s. and, therefore, the ratio $-\dot{h}/2\theta_{DE}$ shall exceed unity. At horizon crossing such ratio must approach unity and keep to such value as $t$ grows greater than $L$.

This point can also be numerically inspected. In Fig. 12, the ratio $-\dot{h}/2\theta_{DE}$ is plotted against $a$, for those $k$ values which yield the top contribution to the $l$ harmonics indicated in the figure, in the case of a RP model. Clearly, about horizon crossing, $\theta_{DE}$ is already quite close to $-\dot{h}/2$.

The main differences between open and dynamical DE models, in the r.h.s. of eqs. (5.5) are therefore relegated to times before horizon crossing. Afterwards, the residual difference is due to a factor $1+w$. If $w$ is too close to $-1$, however, such factor risks to spoil the similarities noticed hereabove.

The changes in $\dot{\eta}$ directly act on $F_2$. The equation fulfilled by this spectral component reads:

$$\dot{F}_2(k,t) = a\, n_e \sigma_T \left[-F_2(k,t) + \frac{\Pi(k,t)}{10}\right] + \frac{k}{5}[2\, F_1(k,t) - 3F_3(k,t)] + \\ + \frac{8}{5}\left(\dot{\eta}(k,t) + \frac{\dot{h}(k,t)}{6}\right) \qquad (5.7f)$$

in flat models, while in open models we have:

$$\dot{F}_2(\beta,t) = a\, n_e \sigma_T \left[-F_2(\beta,t) + \frac{\Pi(\beta,t)}{10}\right] + \frac{\beta}{5}[2b_2\, F_1(\beta,t) - 3b_3 F_3(\beta,t)] + \\ + \frac{8}{5}\frac{\beta}{k} b_2 \left(\dot{\eta}(\beta,t) + \frac{\dot{h}(\beta,t)}{6}\right) \ . \qquad (5.7o)$$

Let us recall that $F_2$ is the only term of $\Pi$ where anisotropy contributes. Such contribution is therefore directly affected by a change in the equation of the gravitational field, which describes the ISW effect in the synchronous gauge and can be similar in open models and in models with dynamical DE, provided that $w$ is not too far from -1/3.

Accordingly, when open models show negative TE correlations at low $l$, we can expect the same to occur in flat RP models. On the contrary, SUGRA models, which grant a cosmic acceleration much closer to $\Lambda$CDM models, due

to a $w$ value not too far from -1, should not be expected to give negative TE correlation and cannot be tested in the same way as RP models.

## 6 Conclusions

In this paper we showed that a particular class of dynamical DE models can be fairly safely *falsified* using large angle CMB polarization data. Models with DE due to a scalar field, self–interacting through a RP potential, belong to such class. In general, however, we expect that any model with dynamical DE, yielding $w \sim -1/3$ or just slightly smaller, can be tested through similar data.

Our treatment provides quantitative predictions for the case of RP potentials, with the simplest possible reionization history yielding $\tau = 0.08$ or 0.16. If the reionization history was more complicated, as is however likely, quantitative conclusions do not apply and is hard to parametrize the whole functional parameter space, providing precise predictions. An analysis of $TE$ correlation spectra, however, shows that negative values are a generic feature, at low $l$, for most reionization histories. Accordingly, in the absence of such negative signal, a RP model is however disfavored.

An experiment to detect CMB polarization with a resolution of $\sim 7^o$ and $\sigma^P_{pix} \simeq 1\,\mu$K is fully realistic. With such noise, there is a substantial fraction of realizations of a RP model with $\Lambda = 10^6\,$GeV, with $\tau = 0.16$, which can be distinguished from $\Lambda$CDM at the 3–$\sigma$ level. Accordingly, the data analysis of a polarization experiment, with a noise level of $\sim \sigma^P_{pix} = 1\,\mu$K, has, at least, $\sim 30\,\%$ of probability to indicate that the model is RP, if this is true. At the 2–$\sigma$ level, such model could be confused with $\Lambda$CDM only in quite a small fraction of realizations.

The only planned polarization experiment specifically aiming to large angle polarization data is SPOrt. The noise level that SPOrt now expects is not much more than $1\,\mu$K per pixel. Other experiments, planned to provide data with greater resolution, can also provide large–angle harmonics. For instance, the WMAP satellite, although not built to minimize systematic effects on polarization, can be able to provide polarization data with a noise level just slightly worse than SPOrt, so allowing an earlier test of RP models. Finally, with the sensitivity expected for PLANCK, RP and similar models can be surely tested.

In order to determine the energy scale $\Lambda$ for RP potentials or to distinguish between $\Lambda$CDM from other DE potentials, using large angular scale data, a pixel noise even below $0.1\,\mu$K is apparently required. No planned polarization experiment will achieve such noise level soon and we can expect that an in-

sight on the shape of DE potentials can come earlier from different kinds of experiments.

## 7 Note added after WMAP release

After submission of this paper and during its revision following the referee report, the first release of WMAP data occurred [6]. This suggests to add some further comments.

Apparently WMAP data give no indication of $C_l^X$ being negative. The three procedures, used to estimate it, all yield large $C_l^X$ values at low $l$ and $\tau = 0.16 \pm 0.04$, for $\Lambda$CDM models and a single reionization. One of the above procedures explicitly assumes that a fair approximation to the true model can be found among $\Lambda$CDM models, trying to fix $\Lambda$CDM parameters best fitting data. The $C_l^X$ spectrum was also related its Fourier transform, and then determined with a third procedure claimed to be fully model–independent.

Here we wish to outline that the first procedure is unsuited to exclude RP models. Following the pattern of Sec. 5, we created a set of artificial skies for RP models with $\Lambda = 10^3$GeV and $10^6$GeV and $\tau = 0.16$. We applied the maximum likelihood procedure to these data and fit cosmological parameters, *assuming that the true model is* $\Lambda$CDM. For the sake of example, in Fig. 13 we show the likelihood distribution on $\Omega_\Lambda$, for a RP model with $\Lambda = 10^3$GeV. The procedure, being unable to explore a fair class of models, systematically overestimates $\Omega_{DE}$; if the noise is $\sim 1\,\mu$K, the likelihood distribution is significantly non-Gaussian. When noise is reduced, the likelihood distribution is more Gaussian, but still peaks at high $\Omega_{DE}$. Then, for $\sigma_{pix}^P = 0.1\,\mu$K, the Gaussian becomes very narrow and the fair $\Omega_{DE}$ value lies at more than 3–$\sigma$ from the best fitting $\Omega_{DE}$. The situation is similar for $\Lambda = 10^6$GeV.

In Fig. 14, we make use of this latter model to compare the RP spectrum used to create data, with the best–fit $\Lambda$CDM spectrum. The continuous line connects the $C_l^X$ values of the RP model; the long–dashed line yields the $C_l^X$ values for a $\Lambda$CDM model with the right $\Omega_{DE}$; the short–dashed connects the $C_l^X$ values for the best–fit $\Lambda$CDM model, with 1–$\sigma$ error–bars. The shaded area shows the range of the cosmic variance.

For the sake of comparison, Figs. 15 and 16 are analogous to Figs. 13 and 14, but for a SUGRA model. In the absence of the peculiar negative behavior, characterizing the RP case, no misleading effect is present.

[6] `http://lambda.gsfc.nasa.gov/product/map/m_overview.html`

With the reserves that these tests suggest, and relying on the *model independent* $C_l^X$ deduction procedure, we however conclude that WMAP apparently excludes that DE is due to a scalar field, self–interacting through a RP potential with $\Lambda \gtrsim$ 1–10 GeV. We plan to deepen the quantitative aspects of this finding in a forthcoming paper.

Acknowledgements – LPLC acknowledges the financial support of ASI, within the activities related to the SPOrt experiment. The CINECA consortium is thanked for making its facilities available for this work. The components of the SPOrt team are also thanked for discussions on the topics of this research. The public programs CMBFAST, by U. Seljak & M. Zaldarriaga, and HEALPix, by K.M. Gòrski et al. were widely used in the preparation of this work.

## References

Albrecht, A. & Skordis, C. 2000, Phys. Rev. Lett., 84, 2076

Amendola, L. 2000, Phys. Rev. D, 62, 043511

Becker, R.H. et al., 2001, AJ, 122, 6

Brax, P., Martin J. & Riazuelo A., 2000, Phys.Rev. D, 62, 103505

Brax, P. & Martin, J., 1999, Phys.Lett., B468, 40

Brax, P. & Martin, J., 2000, Phys.Rev. D, 61, 103502

Bruscoli, M., Ferrara, A., & Scannapieco, E., 2002, MNRAS, 330, L43

Carretti, E., et al., 2000, in: IAU Symposium 201, New Cosmological Data and the Value of Fundamental Parameters, Astron. Soc. Pacif. Conf. Series, eds. Lasenby A. and Wilkinson A.

Colombo, L.P.L. & Bonometto, S.A., 2002, New Astr. 8, 313

Djorgovski, S.G., Castro, S.M., Stern, D. & Mahabal, A.A., 2001, ApJ, 560, L5

Dolgov A.D., 2002, Invited Review Talk given at the VII Workshop on Topics in Astroparticle and Underground Physics (TAUP2001), Sept. 2001, L.N. Gran Sasso, Italy, astro-ph/0201107

Efstathiou, G., et al., 2002, MNRAS, 330, L29

Ferreira, P.G. & Joyce, M. 1998, Phys. Rev. D, 58, 023503

Gnedin, N.Y. & Ostriker, J.P. 1997, ApJ, 486, 581

Haiman, Z., Rees, M.J. & Loeb, A. 1997, ApJ, 484, 985

Haiman, Z., Abel, T. & Rees, M.J.2000, ApJ, 534, 11

Kovac C., Leitch E.M., Pryke C., Carlstrom J.E., Halverson N.W., Holzapfel W.L. 2002, ApJ, in press, astro-ph/0209478

Netterfield, C. B. et al. 2002, ApJ, 571, 604

Ma, C.P. & Bertshinger, E., 1995, ApJ, 455, 7

Macculi, C., et al., 2000, in: What are the Prospect for Cosmic Physics in Italy?, eds. Aiello S. and Blanco A., Conf. Proc. 68, 171.

Miralda-Escudé, J. 2002, ApJ, submitted, astro-ph/0211071

Oh, S.P. 2001, ApJ, 553, 499

Percival, W.J., et al. 2002, MNRAS, in press, astro-ph/0206256

Perlmutter, S., et al. 1998, Nature 391, 51

Perrotta, F. & Baccigalupi, C. 1999, Phys. Rev. D, 59, 123508

Peverini et al., 2001, Int. Workshop on Background Polarized Emission, Bologna, 2001, AIP Conf Proc.

Ratra, B. & Peebles P.J.E., 1988, Phys Rev D, 37, 3406

Pogosian, D., Bond, J.R., & Contaldi, C. 2003, astro-ph/0301310

Riess, A.G., et al 1998, AJ 116, 1009

Steinhardt, P.J., Wang, L., & Zlatev, I. 1999, Phys. Rev. D, 59, 123504

Schuecker P., Caldwell R.R., Boehringer H., Collins C.A. & Guzzo L., 2003 astro-ph/0211480, A&A (in press)

Stompor R. et al, 2001, ApJ, 561, L7

Tegmark, M. et al. 1997, ApJ, 474, 1

Tegmark, M., Zaldarriaga, M., & Hamilton, A. J. 2001, Phys Rev D, 63, 43007

Tucci, M., Carretti, E., Cecchini, S., Cortiglioni, S., Fabbri, R. & Pierpaoli, E., 2000, New Astr., 5, 181

Venkatesan, A., Giraux,M.L. & Shull, J.M. 2001, ApJ, 563, 1

Wetterich, C., 1988, Nucl.Phys.B, 302, 668

Wetterich, C., 1995, A & A, 301, 321

Zaldarriaga, M., 1998, ApJ, 503

Zlatev, I., Wang L. & Steinhardt P.J., 1999, Phys Rev Lett, 82, 896

## Appendix A

Starting from the Lagrangian density for the $\phi$ field, self–interacting through a potential $V(\phi)$, and using Eulero–Lagrange equations, we can work out the equations for the background unperturbed field $\phi$ and its fluctuations $\delta\phi$. The latter reads

$$\ddot{\delta\phi} + 2\frac{\dot{a}}{a}\dot{\delta\phi} + (k^2 + V''a^2)\,\delta\phi + \dot{\phi}\frac{\dot{h}}{2} = 0 \qquad (A1)$$

and we aim to show that this is equivalent to eq. (5.6), that we report here:

$$\theta + \frac{\dot{h}}{2} = -\frac{1}{1+w}[\dot{\delta} + 3\frac{\dot{a}}{a}(c_s^2 - w)\delta] \ . \qquad (A2)$$

An equation equivalent to eq. (A2) is given, for a generic fluid, by Ma & Bertschinger (1955), who derive it from the pseudo–conservation of the energy–momentum tensor $T_{ij}$.

In this Appendix, for the sake of simplicity, we omit the subscript $_{DE}$ to

$$\delta = \frac{\delta\rho_{DE}}{\rho_{DE}} \quad \text{and} \quad \theta = \frac{k^2}{a^2}\frac{\dot{\phi}\,\delta\phi}{\rho_{DE}(1+w)}, \qquad (A3)$$

as well as to the energy density $\rho$ and to the pressure $p$ of DE.

The proof is simpler if we start from eq. (A2) and obtain eq. (A1). Let us first multiply both sides of eq. (A2) by $(1+w)\rho$ and replace $\dot{\delta}$ by

$$\frac{\dot{\delta\rho}}{\rho} - \frac{\dot{\rho}}{\rho}\frac{\delta\rho}{\rho} = \frac{\dot{\delta\rho}}{\rho} + 3\frac{\dot{a}}{a}(1+w)\frac{\delta\rho}{\rho} \ . \qquad (A4)$$

In this way, we obtain

$$\rho(1+w)(\theta + \frac{\dot{h}}{2}) = -\dot{\delta\rho} - 3\frac{\dot{a}}{a}(1+c_s^2)\delta\rho \ . \qquad (A5)$$

Owing to the definition of $\theta$ (eq. A3) and thanks to the relation $(1+w)\rho = \rho + p = \dot{\phi}^2/a^2$, the l.h.s. of eq. (A5) becomes $(k^2/a^2)\dot{\phi}\,\delta\phi + (\dot{\phi}^2/a^2)(\dot{h}/2)$, while, at the r.h.s., we may replace $\delta\rho$ and $\dot{\delta\rho}$ with the expressions obtainable from the definition of $\rho = \dot{\phi}^2/2a^2 + V$. Both sides of the resulting equation must then be divided by $\dot{\phi}/a^2$, so obtaining

$$k^2\delta\phi + \dot{\phi}\frac{\dot{h}}{2} = -\ddot{\delta\phi} - (\frac{\ddot{\phi}}{\dot{\phi}} + a^2\frac{V'}{\dot{\phi}} - 2\frac{\dot{a}}{a})\dot{\delta\phi} - V''a^2\delta\phi - 3\frac{\dot{a}}{a}(1+c_s^2)(\frac{\dot{\phi}\dot{\delta\phi}}{a^2} + V'\delta\phi)\frac{a^2}{\dot{\phi}} \ . \qquad (A6)$$

Here we ought to use the equation of motion of the unperturbed field $\phi$, which can be easily reset to yield that $\ddot{\phi}/\dot{\phi} = -2\dot{a}/a - a^2V'/\dot{\phi}$. Rearranging the

terms, we then obtain:

$$\ddot{\delta\phi} + 2\frac{\dot{a}}{a}\dot{\delta\phi} + (k^2 + V''a^2)\,\delta\phi + \dot{\phi}\frac{\dot{h}}{2} = 3\frac{\dot{a}}{a}[(1-c_s^2)\dot{\delta\phi} - (1+c_s^2)a^2\frac{V'}{\dot{\phi}}\delta\phi]\ . \quad (A7)$$

Eq. (A7) coincides with the equation of motion (A1), provided that the r.h.s. vanishes. This follows the very definition of sound velocity

$$c_s^2 = \frac{\delta p}{\delta\rho} = \frac{\dot{\phi}\dot{\delta\phi}/a^2 - V'\delta\phi}{\dot{\phi}\dot{\delta\phi}/a^2 + V'\delta\phi} \quad (A8)$$

from which we easily obtain that $(1+c_s^2)/(1-c_s^2) = \dot{\phi}\dot{\delta\phi}/a^2V'\delta\phi$. This last relation clearly yields the vanishing of the r.h.s. of eq. (A7).

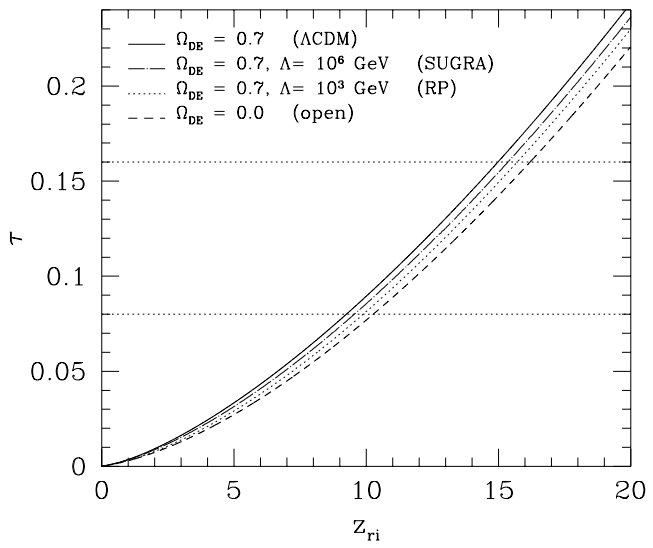


Fig. 1. Optical depth to CMB photons, in different models with $\Omega_m = 0.3$, $h = 0.7$ and $\Omega_b h^2 = 0.022$, as a function of the reionization redshift $z_{ri}$. The two horizontal dotted lines show the reionization redshift consistent with $\tau = 0.08$ or 0.16, in the case of a single, fast and complete reionization event.

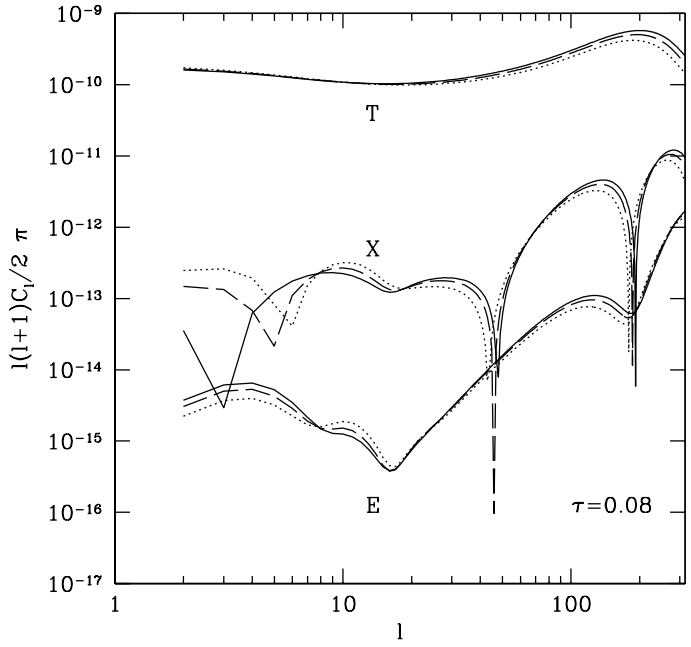


Fig. 2. Angular spectra of RP models with $\tau = 0.08$. Continuous (dashed, dotted) lines correspond to $\Lambda = 10^3$ $(10^6, 10^9)$GeV. The absolute values of $C_l^X$ is plotted; changes of sign are indicated by cusps; notice cusps at low $l$.

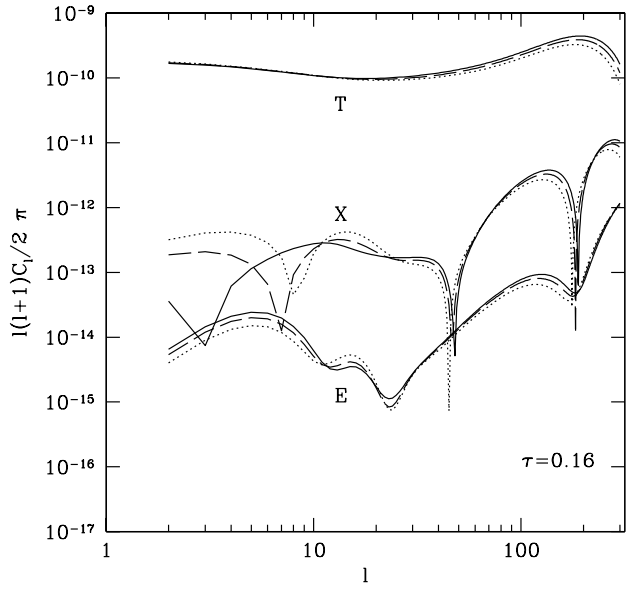


Fig. 3. As Fig. 2, but for $\tau = 0.16$.

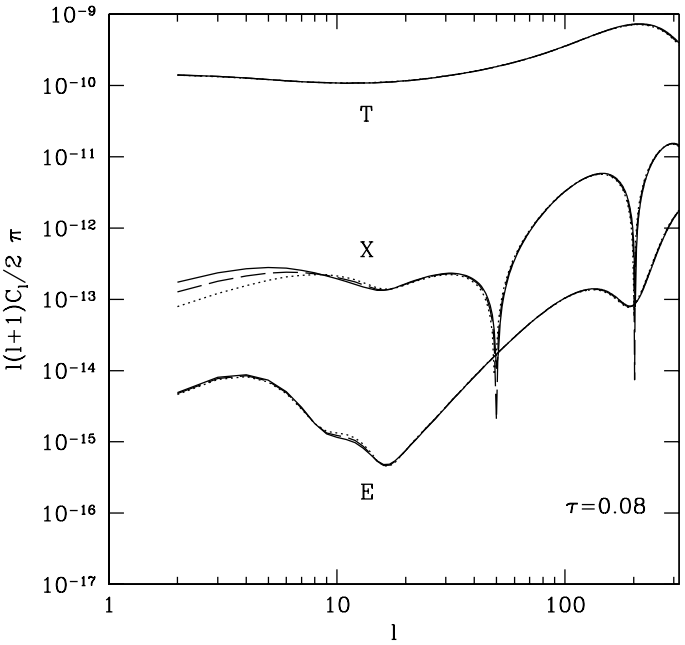


Fig. 4. As Fig. 2, but for SUGRA potentials. Also for SUGRA potentials, the main dependence on the energy scale $\Lambda$ concerns the spectrum $C_l^X$ at quite low $l$. This dependence is however much milder than for RP potentials.

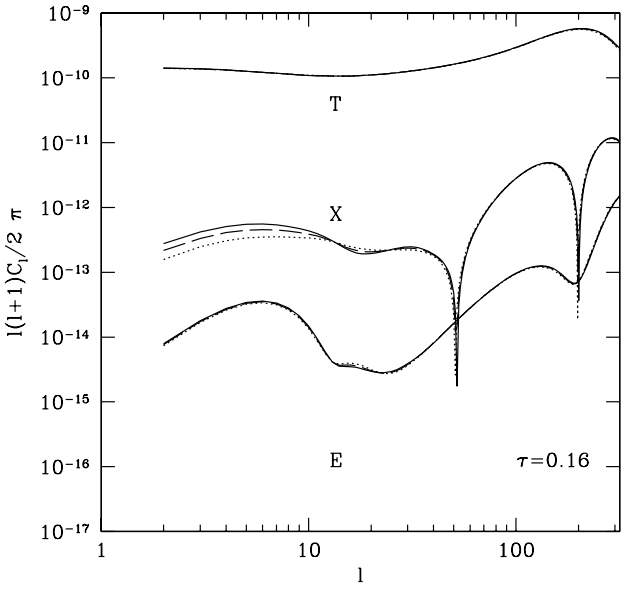


Fig. 5. As Fig. 4, but for $\tau = 0.16$.

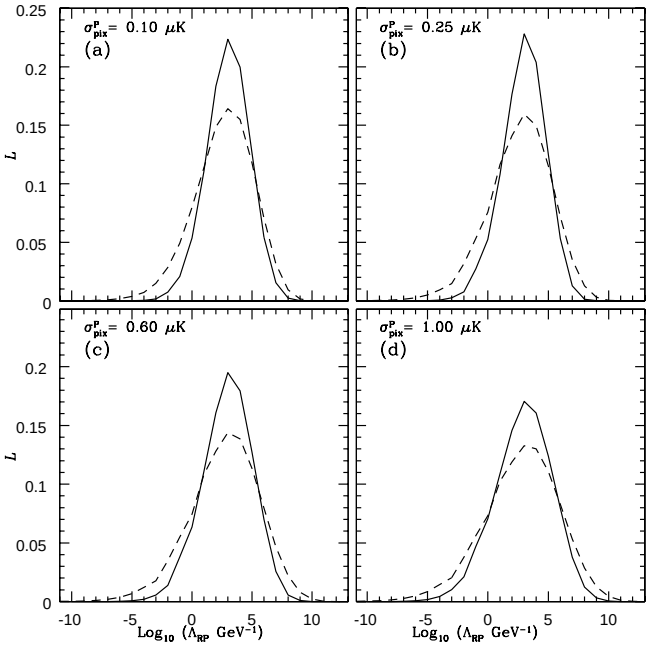


Fig. 6. The likelihood of various energy scales $\Lambda$ is determined from artificial data, created for a model with given $\Lambda$ and for an instrument measuring polarization with given $\sigma^P_{pix}$ (indicated in the frames). In these plots $\Lambda = 10^3$GeV, continuous (dashed) lines refer to models with $\tau = 0.16$ (0.08). The curves give the likelihood obtained averaging among 1000 model realizations. Even with $\sigma^P_{pix} \simeq 0.1\,\mu$K, there is a significant likelihood for $\Lambda < 1$ GeV. See Figs. 11 to relate such likelihood to the fraction of realizations for which the model cannot be distinguished from $\Lambda$CDM.

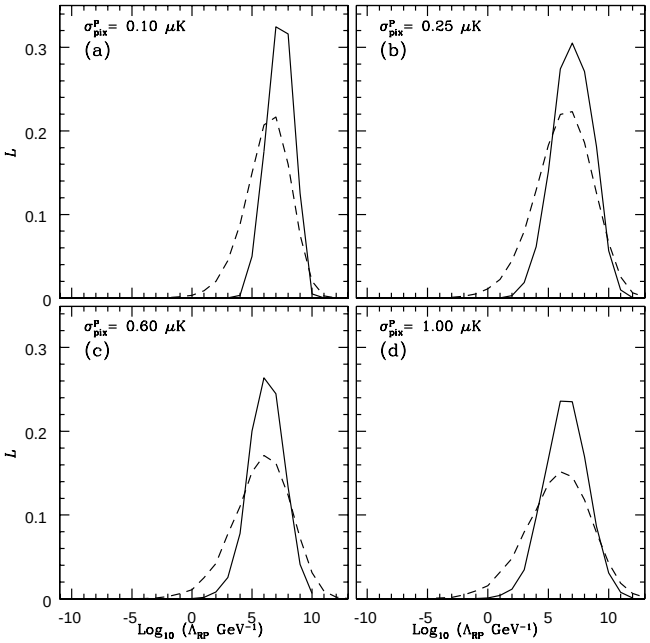


Fig. 7. The same as Fig. 6, but for $\Lambda = 10^6$GeV. Such model is only in marginal agreement with data on SNIa.

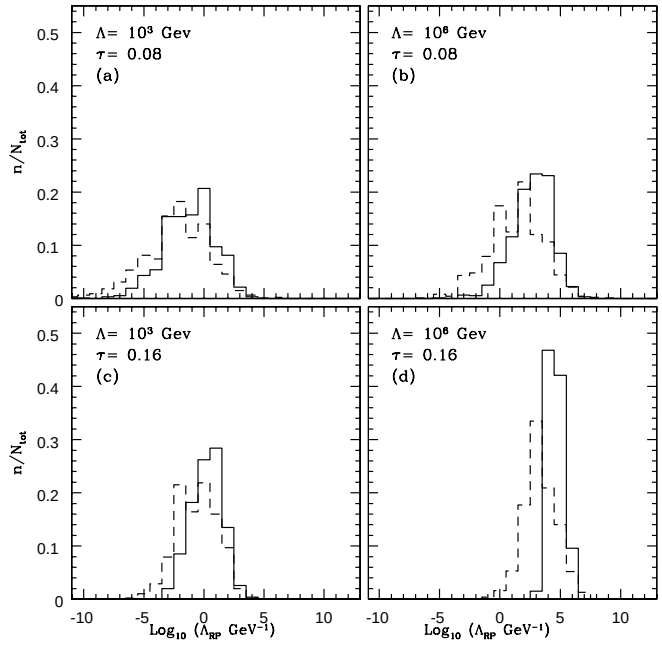


Fig. 8. In this (and the following) plot(s) we describe the effects of cosmic variance, showing how 1–$\sigma$ lower limits on $\Lambda$ depend on the model realization. The continuous (dashed) curve refer to $\sigma^P_{pix} = 0.1$ (1) $\mu$K. In the frames, the values of the energy scale $\Lambda$ and of the opacity $\tau$ are indicated. Notice that, even in the worst case, there is a substantial fraction of realizations which allow to set a limit $\Lambda \gtrsim 1\,\mathrm{GeV}$, so distinguishing a RP model from $\Lambda$CDM. For $\Lambda = 10^6$GeV and $\tau = 0.16$, the fraction of realizations indistinguishable from $\Lambda$CDM, with the reasonable noise level $\sigma^P_{pix} = 1\,\mu$K, is $\sim 2\,\%$.

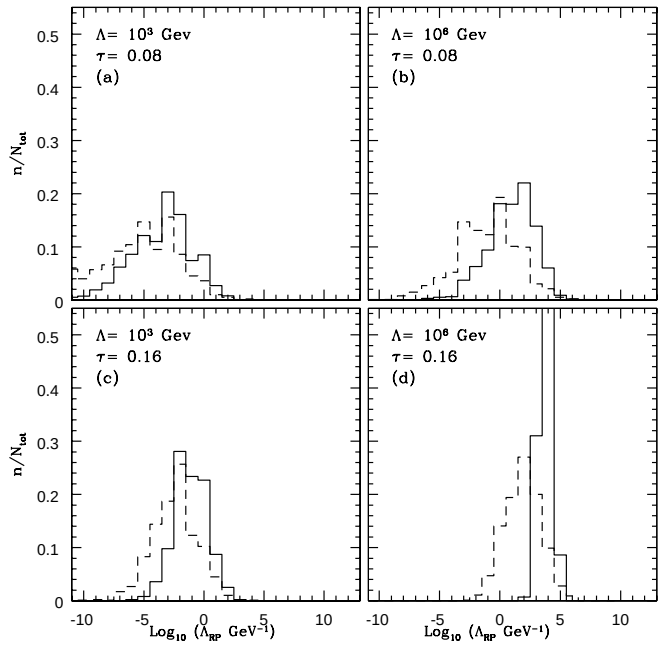


Fig. 9. As Fig. 8, at the 2–$\sigma$ confidence level. For $\Lambda = 10^6$GeV and $\tau = 0.16$, the fraction of realizations indistinguishable from $\Lambda$CDM, with $\sigma^P_{pix} = 1\,\mu$K, is $\sim 16\,\%$.

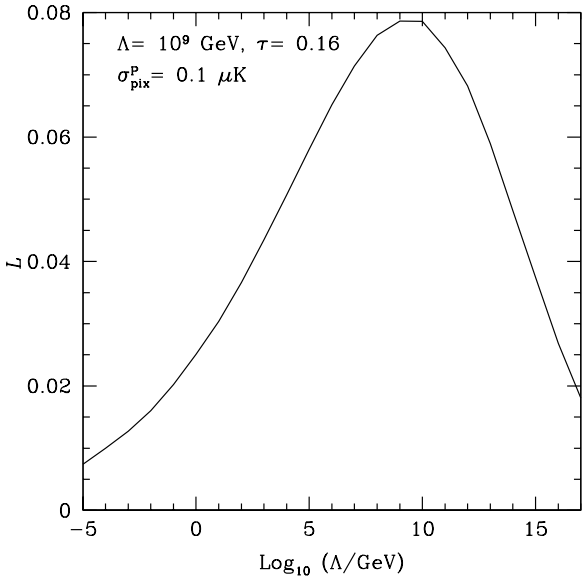


Fig. 10. This figure is analogous to Fig. 6 and concerns the SUGRA model for which $\Lambda$ is best determined by artificial data. The pixel noise is 10 times smaller than the most optimistic expected noise for SPOrt. This plot is obtained by averaging over 1000 realizations.

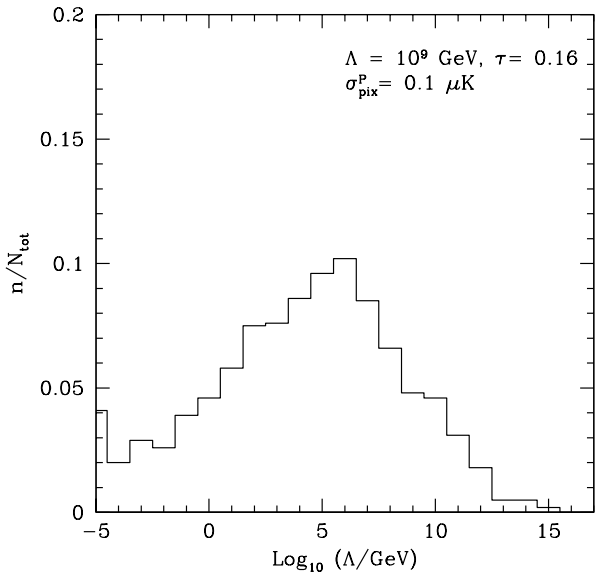


Fig. 11. 1–$\sigma$ lower limit distribution for the SUGRA model for which $\Lambda$ is best determined by artificial data.

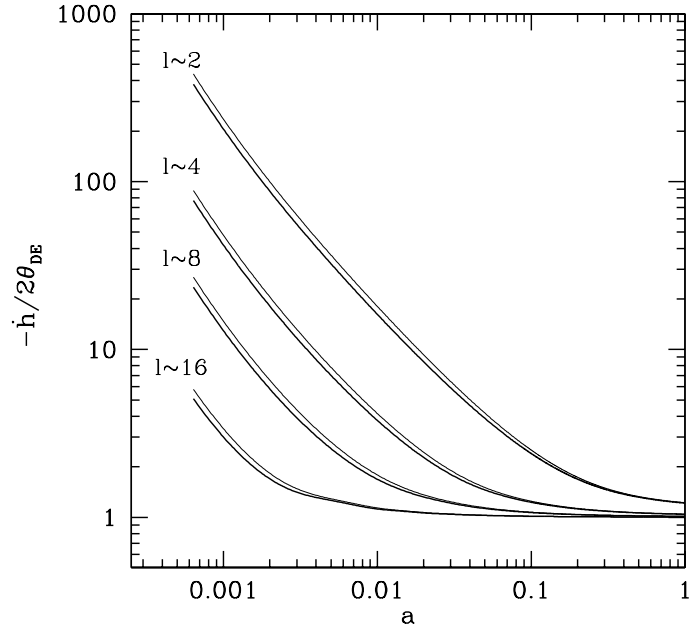


Fig. 12. The ratio $-\dot{h}/2\theta_{DE}$ is plotted with a thick (thin) line for RP models with $\Lambda = 10^3(10^6)$GeV

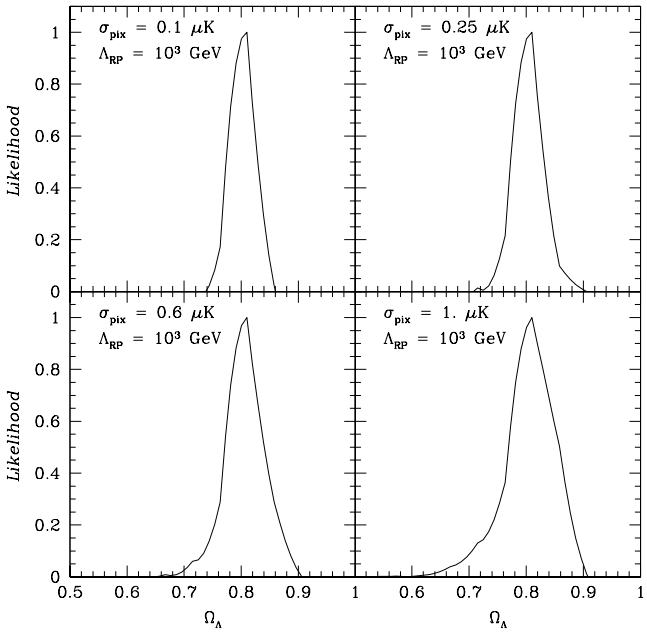


Fig. 13. Likelihood distribution on $\Omega_{DE} \equiv \Omega_\Lambda$, when RP artificial data are fitted with ΛCDM models. RP model parameters are shown in the frames. In all cases the true model has $\Omega_{DE} = 0.7$.

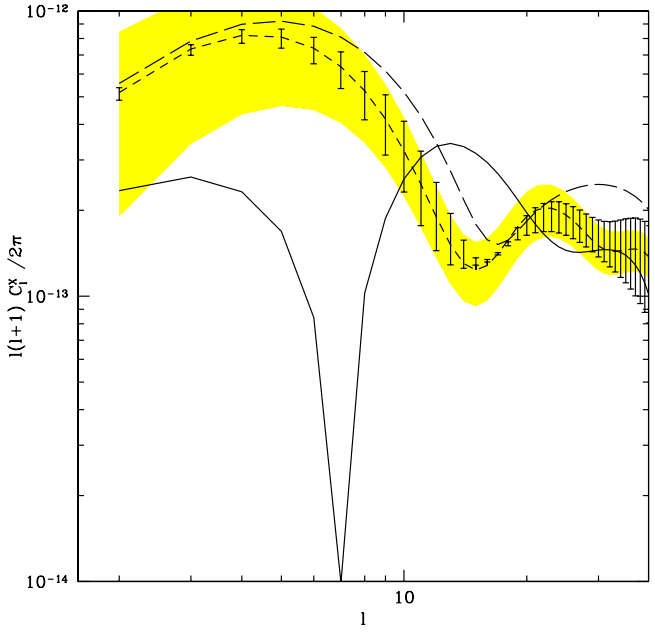


Fig. 14. $C_l^X$ spectrum of the ΛCDM model best fitting RP model data with $\Lambda = 10^6$GeV. See text for more details.

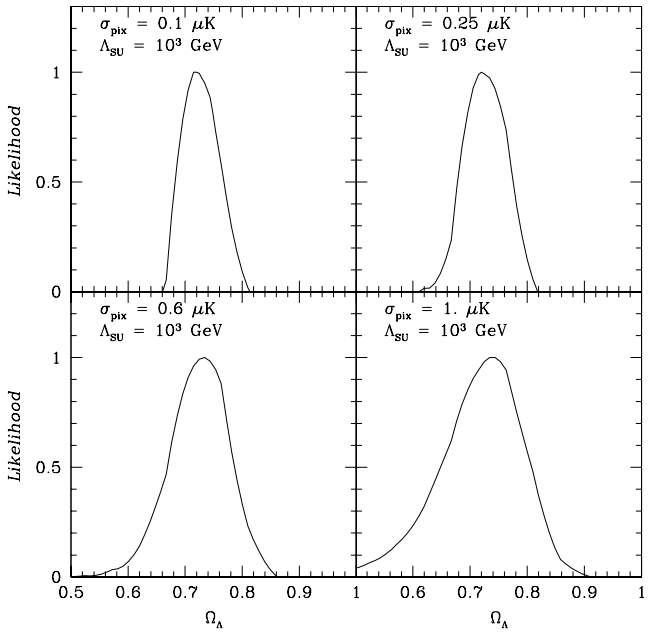


Fig. 15. Likelihood distribution on $\Omega_{DE}$, when SUGRA artificial data are fitted with $\Lambda$CDM models. In this case, the model parameters, shown in the frames, are well approached.

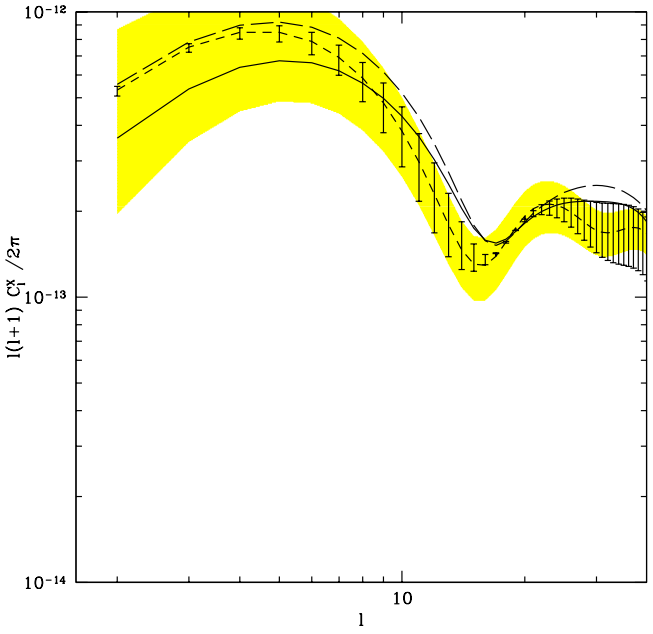


Fig. 16. $C_l^X$ spectrum of the $\Lambda$CDM model best fitting SUGRA model data with $\Lambda = 10^3$GeV. See text for more details. In this case, thanks to the lack of negative $TE$ correlation, the fitting procedure has no serious misleading effect.